arXiv:1201.4097v3 [quant-ph] 24 Feb 2012

Quantum storage of polarization qubits in birefringent and anisotropically absorbing materials

Christoph Clausen, Félix Bussières, Mikael Afzelius,[*] and Nicolas Gisin
Group of Applied Physics, University of Geneva, CH-1211 Geneva 4, Switzerland

(Dated: February 27, 2012)

Storage of quantum information encoded into true single photons is an essential constituent of long-distance quantum communication based on quantum repeaters and of optical quantum information processing. The storage of photonic polarization qubits is, however, complicated by the fact that many materials are birefringent and have polarization-dependent absorption. Here we present and demonstrate a simple scheme that allows compensating for these polarization effects. The scheme is demonstrated using a solid-state quantum memory implemented with an ensemble of rare-earth ions doped into a biaxial yttrium orthosilicate (Y_2SiO_5) crystal. Heralded single photons generated from a filtered spontaneous parametric downconversion source are stored, and quantum state tomography of the retrieved polarization state reveals an average fidelity of $97.5 \pm 0.4\%$, which is significantly higher than what is achievable with a *measure-and-prepare* strategy.

PACS numbers: 03.67.Hk, 42.50.Ex, 42.50.Md, 42.50.Gy

Optical quantum memories [1] allow storage of quantum coherence and entanglement through the reversible mapping of quantum states of light onto matter. They are an essential component of long-distance quantum communication schemes based on quantum repeaters [2] and of distributed quantum networks [3]. An important property of quantum memories is the ability to operate with true single photons (i.e. single-photon Fock states). Single-photon qubits can be encoded using various degrees of freedoms, such as temporal modes or polarization. Polarization qubits are often employed, owing to the simplicity in performing arbitrary single-qubit gates and projection measurements. Yet, the storage of a qubit in an arbitrary state of polarization is generally complicated by the fact that many quantum memories are birefringent and have a polarization-dependent absorption, e.g. with solid-state devices. This not only leads to an efficiency that depends on the state to be stored, but also introduces a state dependent polarization transformation. Means to avoid this drawback were investigated with memory-specific approaches [4–9] based on polarization-selection rules of suitably chosen atomic transitions. Another approach, that can in principle work for any type of quantum memory, is based on the embedding of two quantum memories into the arms of an interferometer [10–12], which inevitably requires long-term interferometric stability.

In this Letter, we present a simple and stable storage scheme for polarization qubits. We experimentally demonstrate our scheme using birefringent crystals doped with rare-earth ions [13]. In recent years, this type of quantum memory experienced rapid progress and key features were demonstrated, such as long storage times [14], high-efficiency storage [15] and large temporal multi-mode capacity [16, 17]. Operation at the single photon level was demonstrated [18] using the atomic frequency comb protocol [19]. This recently lead to the storage of time-bin entangled photons generated from spontaneous parametric downconversion [20, 21] and to the heralded creation of entanglement shared between two crystals [22]. Here, we experimentally show that they can also faithfully store polarization qubits encoded in heralded single photons, despite their inherent birefringence and absorption anisotropy. Our scheme can in principle work for all photon-echo based quantum memories, independent of the material used for the implementation.

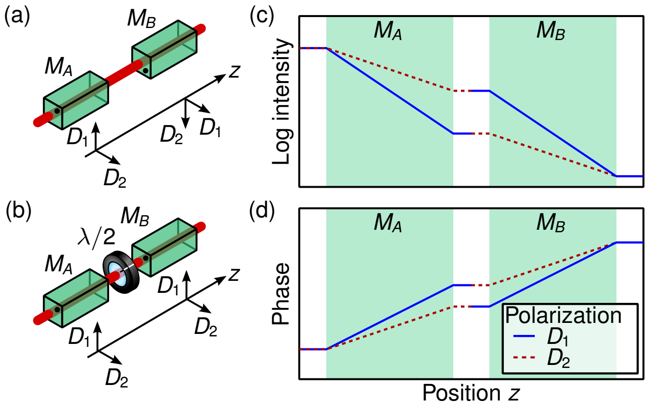

FIG. 1. Scheme for compensating birefringence and absorption anisotropy using two identical quantum memories M_A and M_B. (a) Light propagates along $+z$. The principal axes of the index of refraction D_1 and D_2 of each crystal are orthogonal to z, and M_B is rotated 90° around z with respect to M_A. This arrangement creates a quantum memory that is polarization-preserving and has a constant efficiency for all input polarization states. (b) Alternatively, a wave plate can be inserted between M_A and M_B. (c) Intensity transmitted along the two-memory arrangement of (a) and (b) for light polarized along D_1 or D_2. The total transmission is the same for both components, and hence for any linear combination. (d) The accumulated optical phase for both polarization components along the two-memory arrangement.

Our scheme is illustrated in Fig. 1a using two identical quantum memories M_A and M_B of length L each. Both memories are placed along the z-axis such that their input facet is oriented to contain two of the principal axes of the index of refraction, which we label D_1 and D_2, and M_B is rotated at 90° (around z) with respect to M_A. Light propagates along $+z$ and hits the memories at normal incidence. We assume that the principal axes of absorption coincide with D_1 and D_2. We denote α_1 (or α_2) the absorption coefficient along D_1 (or D_2), and $d_1 = \alpha_1 L$ (or $d_2 = \alpha_2 L$) the associated optical depth. The coincidence between the principal axes of index of refraction and absorption is satisfied by many types of quantum memories, such as rare earth-ions-doped crystals of high symmetry [23]. Hence, the two linear polarizations states parallel to D_1 and D_2 are eigenstates of each memory and form an orthonormal basis that we use to decompose an arbitrary polarization state. Inside M_A, the components will experience different absorption and phase shifts such that an arbitrary polarization input state undergoes a non-unitary transformation stemming from the combined effect of birefringence and absorption anisotropy [24]. Nevertheless, the two-memory configuration is such that after passing through both M_A and M_B, both components experience the same total absorption and global phase shift, and the arrangement is uniformly absorbing and polarization-preserving. Using a rigorous decomposition of the whole memory into infinitesimal longitudinal elements, we can show that the memory efficiency of the forward re-emitted light can be the same for all polarizations, and that the polarization is preserved (see Appendix). The same conclusion holds with the configuration of Fig. 1b where, instead of rotating M_B, a half-wave plate inserted between M_A and M_B swaps the eigenstates (here, the output polarization is preserved up to the swap operation).

We note that the high fidelity of our scheme is conditioned on the interferometric stability of the distance between the two memories, but only on the time scale of the storage time. This condition is experimentally simple to satisfy, especially if the two memories are mounted in a spatial configuration yielding common mode rejection of vibration. In particular, this is easier to satisfy than the long-term stability over the ensemble of all measurements that is required for the scheme based on memories embedded in a Mach-Zehnder interferometer [10–12].

We shall now present a series of measurements made with a pair of 1 cm long Nd^{3+}:Y_2SiO_5 crystals for which we explicitly verified that the principal axes of the index of refraction and of absorption coincide. We stress that the host biaxial crystal is highly birefringent, with a polarization beat length on the order of 100 µm at 883 nm [25]. First, we show that the dependence of the optical depth on the polarization of the light can be strongly attenuated. As a consequence, the efficiency of the quantum memory is practically constant. Second, we use the quantum memory for storage and retrieval of heralded single photons with several polarizations, and obtain the fidelity of the storage process using quantum state tomography.

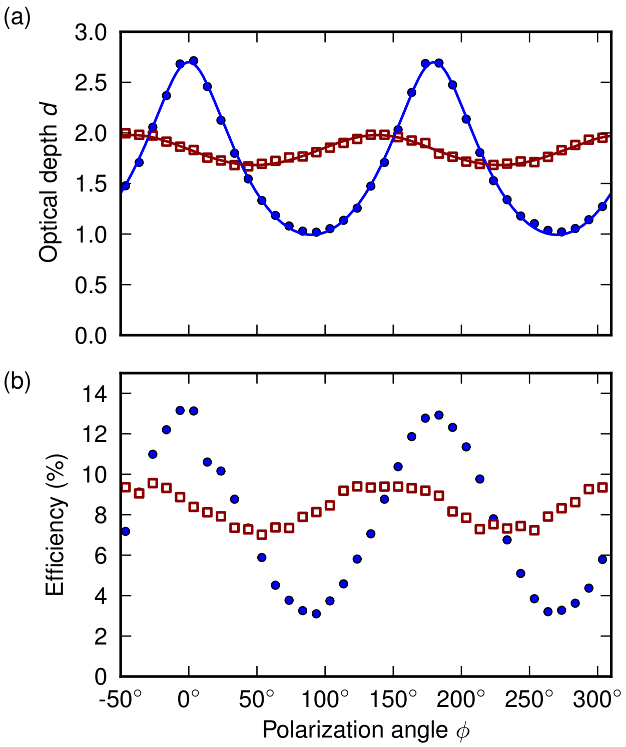

FIG. 2. Measurements of (a) optical depth and (b) memory efficency of two Nd^{3+}:Y_2SiO_5 crystals without (●) and with (□) compensation scheme. Incident light is linearly polarized, and the x-axis indicates the angle of the polarization with respect to the D_1 axis of the crystals. (a) Without compensation the optical depth varies between 2.70(1) and 0.99(1), corresponding to propagation along the two optical extinction axes. With compensation the peak-to-peak variation is reduced to 16% of the mean optical depth. Lines are fits to Eq. (1). (b) Efficiency of 50 ns storage measured using laser pulses. With compensation the efficiency is almost independent of polarization.

We first measured the total optical depth d on the $^4I_{9/2} \rightarrow {}^4F_{3/2}$ transition at 883 nm of the pair of Nd^{3+}:Y_2SiO_5 crystals, cooled down to 3 K, while varying the polarization of the incident light. The optical depth is obtained through $P_{\text{out}} = P_{\text{in}} e^{-d}$, where P_{in} (or P_{out}) is the optical power before (or after) the two crystals. The two crystals were initially in the configuration of Fig. 1b, but without the wave plate between the crystals. The measured optical depth is shown in Fig. 2a. Without the compensation scheme, the absorption varies strongly with the linear polarization state, as expected. The overall absorption for any linear polarization can be calculated by decomposing the light into its components along the two principal axes, such that the overall optical depth is given by [26],

$$d = -\ln\left(e^{-d_1}\cos^2\phi + e^{-d_2}\sin^2\phi\right), \qquad (1)$$

where d_1 (or d_2) is the optical depth for polarization along D_1 (or D_2), and ϕ the angle of the linear polarization with respect to D_1. A fit of the data to Eq. (1) results in values $d_1 = 2.70(1)$ and $d_2 = 0.99(1)$. These values are consistent with previous measurements on a single crystal [16]. We then repeated the measurement using the compensation scheme of Fig. 1b. With compensation, the minimum and maximum values of the optical depth, obtained from another fit to Eq. (1), were found to be 1.68(1) and 1.98(1). We believe that the residual variation can be attributed to birefringence induced by the windows on the cryostat, slight misalignment of the crystals with respect to each other, or unequal crystal lengths. Additionally, it is possible that the retardance and orientation of the half-wave plate deviated from the ideal values.

The optical depth is important for the efficiency of the quantum memory. In the case of the atomic frequency comb, the efficiency varies as $\eta \propto \tilde{d}^2 e^{-\tilde{d}}$, where $\tilde{d} = d/F$ is the average optical depth of the comb, including a dependence on the comb finesse F [19]. This means that variations in the optical depth translate directly to variations in the memory efficiency. We verified this using the same setup as for the measurement of the optical depth, but now the crystals were prepared as 120 MHz wide atomic frequency combs with a preprogrammed storage time of 50 ns (see [20, 22] for details). Using laser pulses of roughly Gaussian shape with 18 ns full width at half maximum, we measured the memory efficiency, that is, the ratio of the area of the retrieved pulse to that of the input pulse, as a function of polarization. Figure 2(b) shows that the efficiency follows the same trend as the optical depth, varying from 3% to 13% without, and from 7% to 9.5% with compensation.

Let us now turn to the storage and retrieval of polarization qubits. The complete setup for this purpose is shown in Fig. 3. The experimental cycle consists of two phases of 15 ms each. In the first phase the inhomogeneous absorption of the two crystals is shaped into an atomic frequency comb by optical pumping during 11 ms (see [20] for details). A waiting time of 4 ms is added to avoid fluorescence from atoms left in the excited state. In the second phase the storage, retrieval and analysis of polarization qubits, encoded on heralded single photons, is performed. Our photon source is described in detail elsewhere [20, 22]. Photon pairs are generated by spontaneous parametric down-conversion in a periodically poled waveguide. The signal and idler photons with wavelengths 883 nm and 1338 nm, respectively, are separated and strongly filtered to match the bandwidth of the quantum memories. The detection of an idler photon heralds the presence of a signal photon, which will act as the polarization qubit. The signal photon then passes through a fiber-based polarization controller, a half-wave plate and a quarter-wave plate to prepare the state of the qubit to be stored. The output of the quantum memory is sent towards a polarization analyzer consisting of a quarter-wave plate, a half-wave plate, a polarizing beamsplitter and two silicon-based single photon detectors. The light that prepares the atomic frequency comb passes through the same waveplates as the single photons. We adjust the polarization of the preparation light using a fiber-based polarization controller, such that it always has the same polarization, independent of the polarization of the photons to be stored.

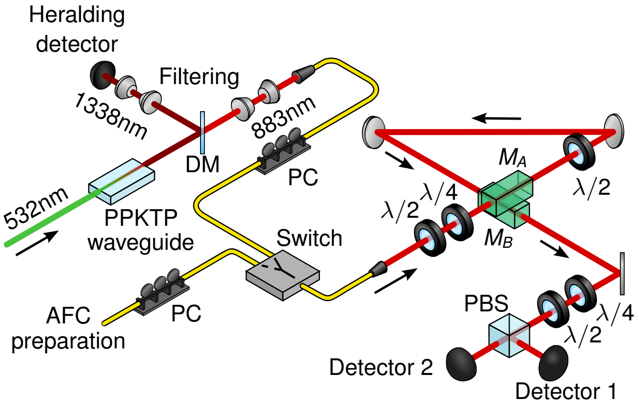

FIG. 3. Experimental setup for polarization qubit tomography. Pairs of photons are generated by spontaneous parametric down-conversion in a periodically poled KTP waveguide pumped with 4 mW of light from a continous-wave laser at 532 nm, separated by a dichroic mirror (DM) and strongly filtered. The detection of a photon at 1338 nm on a superconducting nanowire single photon detector heralds the presence of a photon at 883 nm. The latter is in resonance with the quantum memories M_A and M_B and acts as a polarization qubit. The initial state of the qubit is prepared using a fiber-based polarization controller (PC) and two waveplates ($\lambda/2$ and $\lambda/4$). An effective half-wave plate, made of two quarter-wave plates between the crystals, compensates for their anisotropy. Finally, the polarization state of the retrieved photon is analyzed using two more waveplates ($\lambda/4$ and $\lambda/2$) and a polarizing beamsplitter (PBS) with a silicon avalanche photo diode at each output. Another polarization controller is used to ensure that the quantum memory is always prepared with the same polarization, independent of the polarization state of the photons to be stored.

To show that our compensation method allows for faithful storage of polarization qubits, we performed quantum state tomography [27] on a set of five different input states. The results are shown in Table I. For each tomographic reconstruction we performed measurements along the three principal axes of the Poincaré sphere, and all detections were conditioned on the simultaneous detection of an idler photon.

Based on the measured number of coincidences, we reconstructed the density matrix of the retrieved qubit

Input State	Fidelity	$\bar{g}_{si}^{(2)}$
$\vert H\rangle$	99.3(6)%	7.6(3)
$\vert V\rangle$	97(1)%	6.0(3)
$\vert L\rangle$	97.7(6)%	9.4(3)
$\vert +\rangle$	95(1)%	8.0(3)
$\alpha\vert H\rangle + \beta\vert V\rangle$	98.7(9)%	9.2(3)

TABLE I. Results of the measurements performed on the stored and released single photons for various input states. The fidelity was found via tomographic state-reconstruction using a maximum likelihood method, and the errors estimated via Monte-Carlo simulation. Additionally, the cross-correlation between signal and idler photons $\bar{g}_{si}^{(2)}$, averaged over measurement settings and detectors, indicates the quantum character of the process. The fifth input state is obtained by sending $|H\rangle$ through a quarter-wave plate oriented such that $\alpha = (1 + i\sqrt{2})/2$ and $\beta = 1/2$.

by maximum likelihood estimation [27]. The fidelity with respect to the input state is shown in Table I. We also estimated the uncertainty on the fidelity using a Monte-Carlo simulation based on the Poissonian statistics of the detection events. In all cases we find fidelities $F \gtrsim 95\%$, which significantly surpasses the limit of 2/3 of any classical memory based on a *measure-and-prepare* strategy [28]. This proves that we have implemented a quantum memory that preserves arbitrary states of polarization to a high degree. We attribute the deviation from unit fidelity to imperfections in the state preparation, anisotropy compensation and analysis, caused by non-ideal wave plates.

Finally, we investigated the quantum nature of the storage process. First, a measurement of the zero-time auto-correlation function of the heralded signal photon (before storage) yielded $g_{s|i}^{(2)} < 0.06$, which confirms the single-photon nature of the polarization qubit to be stored. The non-classicality of the photon retrieved from the memory can then be revealed with another measurement, namely the zero-time intensity cross-correlation $g_{si}^{(2)}$ between signal and idler fields. Specifically, assuming auto-correlations $g_x^{(2)}$ for signal and idler fields of $1 \leq g_x^{(2)} \leq 2$, where $x =$'s' for signal and 'i' for idler, the signature of non-classicality between both fields becomes $g_{si}^{(2)} > 2$ [29]. We measured values between $\bar{g}_{si}^{(2)} = 6.0(3)$ and $\bar{g}_{si}^{(2)} = 9.4(3)$ for all the stored polarization states, confirming the quantum nature of the storage and retrieval process. The lowest cross-correlation value allows to upper bound the auto-correlation of the retrieved signal photon to $g_{s|i}^{(2)} \leq 0.61(3)$, which is still below the classical threshold of 1 (the upper bound is obtained by assuming that the source is exactly described by a two-mode squeezed state [22]). We note that the relatively large increase of $g_{s|i}^{(2)}$ before and after storage is almost entirely due to an experimental artifact associated with the continuous wave operation of our source of photon pairs [22], and not to a detrimental effect stemming from the memory itself.

To conclude, we have experimentally demonstrated a scheme that allows the faithful storage of polarization qubits encoded into true single photons using a material that is birefringent and has anisotropic absorption. We note that the efficiency of a photon-echo based quantum memory with re-emission in the forward mode is limited to 54% [19, 30]. To overcome this limitation, and possibly reach 100% efficiency, one possibility is to use the impedance-matched quantum memory scheme in which a forward-emitting quantum memory is placed between two-mirrors with reflectivity chosen such that all the incident light can be absorbed and re-emitted [31]. Our scheme thus has the potential for demonstrating a high-efficiency solid-state quantum memory that is compatible with polarization qubits. It is particularly well-suited for rare-earth-ions-doped crystals and greatly extends their range of application. For example, the storage of both polarization and temporal modes leads to new interesting possibilities, such as the quantum storage of hyperentangled photons [32].

We thank Imam Usmani, Nicolas Sangouard and Philippe Goldner for stimulating discussions. We acknowledge support by the Swiss NCCR Quantum Photonics, the Science and Technology Cooperation Program Switzerland-Russia, as well as by the European projects QuRep and ERC-Qore. F.B. was supported in part by le Fond Québécois de la Recherche sur la Nature et les Technologies.

We note that related results have been obtained in other groups [33–35].

Appendix

We here present a detailed theoretical description of our scheme for compensating birefringence and anisotropic absorption in quantum memories. We represent the polarization input state in terms of a Jones vector $|\Psi_i\rangle$ that is transformed to an output state $|\Psi_f\rangle = \mathbf{M}|\Psi_i\rangle$, where $\mathbf{M}$ is a 2×2 square complex matrix.

We use the theory derived in [24], which treats the effects of birefringence (or polarization-mode dispersion, PMD) and polarization-dependent loss (PDL). In [24] it is shown that any transformation $\mathbf{M}$ of the input state induced by propagation through a memory having PMD and PDL effects, can be decomposed into a product of an unitary matrix $\mathbf{U}$ describing an effective PMD and an Hermitian positive matrix $\mathbf{T}$ describing an effective PDL:

$$\mathbf{M} = \mathbf{TU}.$$

In the most general case when the principal axes of the PDL and PMD do not coincide, $\mathbf{T}$ and $\mathbf{U}$ do not commute [24]. For rare-earth doped crystals, in most materials commonly used, the principal axes of the absorption coefficient and the index of refraction do coincide due to symmetry considerations. This is the case, for instance, when the dopant site has an axial symmetry. In our crystal, Nd:Y_2SiO_5, the neodymium ions are in a crystallographic site of low symmetry C_1 and Y_2SiO_5 is a biaxial crystal. The principal axes of absorption and birefringence could thus be oriented differently. The data presented in the Letter shows, however, that the principal axes do coincide (at least in the plane perpendicular to the crystallographic b-axis). We will thus consider that $\mathbf{U}$ and $\mathbf{T}$ are diagonal in the same basis. The principal axes of birefringence in Y_2SiO_5 are denoted D_1 and D_2 in the Letter.

The matrices $\mathbf{T}$ and $\mathbf{U}$ can then be written as

$$\mathbf{U} = \begin{pmatrix} 1 & 0 \\ 0 & e^{i\phi} \end{pmatrix} \quad \text{and} \quad \mathbf{T} = \begin{pmatrix} e^{-d_1/2} & 0 \\ 0 & e^{-d_2/2} \end{pmatrix},$$

where d_1 and d_2 are the optical depths along the principal axes D_1 and D_2 and $\phi = k\Delta nL$ is the phase accumulated along axis D_2, relative to D_1, due to birefringence $\Delta n = n_2 - n_1$ (that is the difference between the indices of refraction along D_2 and D_1). It is now easily shown that putting two crystals in series, where the second crystal is rotated 90 degrees with respect to the first, results in the identity transformation multiplied by a global polarization-independent absorption (loss)

$$\mathbf{R}(-90^\circ)\mathbf{TUR}(90^\circ)\mathbf{TU} = e^{-(d_1+d_2)/2}e^{i\phi}\,\mathbf{I}.$$

Here $\mathbf{R}(\alpha)$ is the usual 2×2 rotation matrix, α is the angle of rotation, and $\mathbf{I}$ is the identity matrix. Note that in terms of intensity the fraction of absorbed light is $1 - \exp[-(d_1 + d_2)]$.

We have so far shown that the propagation through the two absorbing crystals preserves the polarization state, and that light is uniformly absorbed (or mapped onto) the crystal. For quantum memories it is of course also important to show that the light state can be retrieved efficiently and that the polarization state of the retrieved light is preserved as well.

We model the quantum memory as a "sum over all trajectories" [19, 30, 31]. Each trajectory corresponds to a conversion from the input mode to the output mode at a particular position z in the absorbing medium. Let us assume that the polarization of the input mode corresponds to a polarization eigenvector of the memory, such that its polarization does not rotate through propagation. Moreover, we consider the case where the input and output modes propagate in the same "forward" direction. In this situation, the square root of the memory efficiency, $\sqrt{\eta}$, can be calculated as (see Eq. (A19) in [19])

$$\sqrt{\eta} = \int_0^L e^{-\alpha z/2}\alpha dz e^{-\alpha(L-z)/2} = \alpha L e^{-\alpha L/2} = de^{-d/2}, \tag{A.2}$$

where α is the absorption coefficient, L the memory length and $d = \alpha L$ is the optical depth. The equation above can be understood in the following way. For each trajectory there is the probability amplitude for the input photon to reach point z in the medium ($e^{-\alpha z/2}$), the probability amplitude for the photon to be absorbed in z and re-emitted later (αdz) and the probability amplitude for the output photon to reach the end of the medium ($e^{-\alpha(L-z)/2}$). All trajectory amplitudes can be added coherently in the far field, leading to the final efficiency formula for "forward" memory read-out. For the specific case of the atomic frequency comb protocol, the reasoning is the same, but the optical depth is replaced with $\tilde{d} = d/F$, where F is the finesse of the comb [19].

The well-known result of Eq. A.2 applies to a single polarization mode. The calculation in our case is more general but nevertheless straightforward. The extension to two polarization modes for one crystal can be done as follows:

$$\mathbf{M}' = \int_0^L \mathbf{T}(L-z)\mathbf{U}(L-z)\begin{pmatrix} \alpha_1 dz & 0 \\ 0 & \alpha_2 dz \end{pmatrix}\mathbf{T}(z)\mathbf{U}(z).$$

where the diagonal matrix in the middle accounts for the conversion efficiency for the two polarization modes. This equation can be simplified extensively:

$$\mathbf{M}' = \int_0^L \begin{pmatrix} e^{-(L-z)\alpha_1/2} & 0 \\ 0 & e^{i\phi}e^{-(L-z)\alpha_2/2} \end{pmatrix}\begin{pmatrix} \alpha_1 dz & 0 \\ 0 & \alpha_2 dz \end{pmatrix}\begin{pmatrix} e^{-z\alpha_1/2} & 0 \\ 0 & e^{i\phi}e^{-z\alpha_2/2} \end{pmatrix} =$$

$$\int_0^L \begin{pmatrix} e^{-(L-z)\alpha_1/2}\alpha_1 dz e^{-z\alpha_1/2} & 0 \\ 0 & e^{i\phi}e^{-(L-z)\alpha_2/2}\alpha_2 dz e^{-z\alpha_2/2} \end{pmatrix} = \begin{pmatrix} d_1 e^{-d_1/2} & 0 \\ 0 & e^{i\phi}d_2 e^{-d_2/2} \end{pmatrix}.$$

The effect of both crystals can now be evaluated by summing the amplitudes of the following two possibilities;

a photon is stored in the first crystal and propagates through the second crystal, or the vice versa

$$\mathbf{R}(-90^\circ)\mathbf{M}'\mathbf{R}(90^\circ)\mathbf{M} + \mathbf{R}(-90^\circ)\mathbf{M}\mathbf{R}(90^\circ)\mathbf{M}' = e^{i\phi}(d_1 + d_2)e^{-(d_1+d_2)/2}\,\mathbf{I}.$$

We conclude that the total transformation of the input to output mode preserves the polarization state and the efficiency is given by the usual formula with an effective optical depth $d_1 + d_2$, as one could have expected. The efficiency in this configuration would thus ultimately be limited to 54% for $d_1 + d_2 \approx 2$ [19]. This assumes, of course, that there is no decoherence during the time spent in the memory. Decoherence can, however, be included by simply multiplying the equation above with the appropriate decoherence factor [30].

It has been shown previously that efficiencies approaching 100% can be achieved in the so-called "backward" read out configuration [19]. Using our scheme, however, it is clear that one cannot in general hope to achieve unit efficiency in the backward direction. This is due to the fact that different trajectories with penetration depth z accumulate different phases, due to the birefringence. In the special case of negligible birefringence ($\phi \approx 0$), but with anisotropic absorption, one can still achieve unit efficiency in the backward read out configuration. The calculation leading to this result is similar to the one presented above.

Another way of reaching 100% efficiency is to put the memory in a moderate-finesse cavity, based on the concept of impedance-matching [31]. That scheme is perfectly suitable for our anisotropy compensation scheme, since for each cavity round trip the memory works in forward emission mode. The results presented above thus apply to this type of memory. There exist thus a method to extend the ideas presented here to unit efficiency quantum memories.

---

[*] mikael.afzelius@unige.ch

[1] A. I. Lvovsky, B. C. Sanders, and W. Tittel, Nat. Photon. **3**, 706 (2009)

[2] N. Sangouard, C. Simon, H. de Riedmatten, and N. Gisin, Rev. Mod. Phys. **83**, 33 (2011)

[3] H. J. Kimble, Nature **453**, 1023 (2008)

[4] D. N. Matsukevich, T. Chaneliere, S. D. Jenkins, S.-Y. Lan, T. A. B. Kennedy, and A. Kuzmich, Phys. Rev. Lett. **96**, 030405 (2006)

[5] F. Carreño and M. A. Antón, Opt. Commun. **283**, 4787 (2010)

[6] H. P. Specht, C. Nolleke, A. Reiserer, M. Uphoff, E. Figueroa, S. Ritter, and G. Rempe, Nature **473**, 190 (2011)

[7] M. Lettner, M. Mücke, S. Riedl, C. Vo, C. Hahn, S. Baur, J. Bochmann, S. Ritter, S. Dürr, and G. Rempe, Phys. Rev. Lett. **106**, 210503 (2011)

[8] D. Viscor, A. Ferraro, Y. Loiko, R. Corbalán, J. Mompart, and V. Ahufinger, J. Phys. B: At. Mol. Opt. **44**, 195504 (2011)

[9] S. Riedl, M. Lettner, C. Vo, S. Baur, G. Rempe, and S. Dürr, "A Bose-Einstein condensate as a quantum memory for a photonic polarization qubit," (2011), arXiv:1112.4733

[10] Y.-W. Cho and Y.-H. Kim, Opt. Express **18**, 25786 (2010)

[11] H. Zhang, X.-M. Jin, J. Yang, H.-N. Dai, S.-J. Yang, T.-M. Zhao, J. Rui, Y. He, X. Jiang, F. Yang, G.-S. Pan, Z.-S. Yuan, Y. Deng, Z.-B. Chen, X.-H. Bao, S. Chen, B. Zhao, and J.-W. Pan, Nat. Photon. **5**, 628 (2011)

[12] D. G. England, P. S. Michelberger, T. F. M. Champion, K. F. Reim, K. C. Lee, M. R. Sprague, X.-M. Jin, N. K. Langford, W. S. Kolthammer, J. Nunn, and I. A. Walmsley, "High-fidelity polarization storage in a gigahertz bandwidth quantum memory," (2011), arXiv:1112.0900

[13] W. Tittel, M. Afzelius, T. Chaneliere, R. Cone, S. Kröll, S. Moiseev, and M. Sellars, Laser & Photonics Review **4**, 244 (2010)

[14] J. J. Longdell, E. Fraval, M. J. Sellars, and N. B. Manson, Phys. Rev. Lett. **95**, 063601 (2005)

[15] M. P. Hedges, J. J. Longdell, Y. Li, and M. J. Sellars, Nature **465**, 1052 (2010)

[16] I. Usmani, M. Afzelius, H. de Riedmatten, and N. Gisin, Nat. Commun. **1**, 12 (2010)

[17] M. Bonarota, J.-L. L. Gouët, and T. Chanelière, New Journal of Physics **13**, 013013 (2011)

[18] H. de Riedmatten, M. Afzelius, M. U. Staudt, C. Simon, and N. Gisin, Nature **456**, 773 (2008)

[19] M. Afzelius, C. Simon, H. de Riedmatten, and N. Gisin, Phys. Rev. A **79**, 052329 (2009)

[20] C. Clausen, I. Usmani, F. Bussières, N. Sangouard, M. Afzelius, H. de Riedmatten, and N. Gisin, Nature **469**, 508 (2011)

[21] E. Saglamyurek, N. Sinclair, J. Jin, J. A. Slater, D. Oblak, F. Bussières, M. George, R. Ricken, W. Sohler, and W. Tittel, Nature **469**, 512 (2011)

[22] I. Usmani, C. Clausen, F. Bussières, N. Sangouard, M. Afzelius, and N. Gisin, "Heralded quantum entanglement between two crystals," (2011), arXiv:1109.0440

[23] M. Born and E. Wolf, *Principles of Optics* (Oxford Pergamon press, 1965)

[24] B. Huttner, C. Geiser, and N. Gisin, IEEE J. Sel. Top. Quant. **6**, 317 (2000)

[25] R. Beach, M. Shinn, L. Davis, R. Solarz, and W. Krupke, IEEE J. Quantum Elect. **26**, 1405 (1990)

[26] M. Afzelius, M. U. Staudt, H. de Riedmatten, N. Gisin, O. Guillot-Noël, P. Goldner, R. Marino, P. Porcher, E. Cavalli, and M. Bettinelli, J. Lumin. **130**, 1566 (2010)

[27] J. B. Altepeter, E. R. Jeffrey, and P. G. Kwiat, "Advances in AMO physics," (Elsevier, 2006) Chap. 3

[28] S. Massar and S. Popescu, Phys. Rev. Lett. **74**, 1259 (1995)

[29] A. Kuzmich, W. P. Bowen, A. D. Boozer, A. Boca, C. W. Chou, L.-M. Duan, and H. J. Kimble, Nature **423**, 731 (2003)

[30] N. Sangouard, C. Simon, M. Afzelius, and N. Gisin, Phys. Rev. A **75**, 032327 (2007)

[31] M. Afzelius and C. Simon, Phys. Rev. A **82**, 022310 (2010)

[32] J. T. Barreiro, N. K. Langford, N. A. Peters, and P. G. Kwiat, Phys. Rev. Lett. **95**, 260501 (2005)

[33] E. Saglamyurek, N. Sinclair, J. Jin, J. A. Slater, D. Oblak, F. Bussières, M. George, R. Ricken, W. Sohler, and W. Tittel, “Conditional detection of pure quantum states of light after storage i a waveguide,” (2011), arXiv:1111.0676

[34] M. Gündoğan, P. M. Ledingham, A. Almasi, M. Cristiani, and H. de Riedmatten, “Quantum storage of a photonic polarization qubit in a solid,” (2012), arXiv:1201.4149

[35] Z.-Q. Zhou, W.-B. Lin, M. Yang, C.-F. Li, and G.-C. Guo, “Realization of reliable solid-state quantum memory for photonic polarization-qubit,” (2012), arXiv:1201.4441